ANTIMONY LEACHING FROM STIBNITE AND COMPLEX ORES[1]

Y.T. John Kwong[2], Allen Pratt,[2] and Gianluigi Botton[2]

Abstract. To shed light on the leaching of Sb from mine wastes containing stibnite, two series of experiments were conducted. In one experiment, polished slabs of a museum-grade stibnite and a mixed-sulfide ore sample containing 28% Sb were subjected to accelerated weathering at 100% humidity and 31-35°C for 37-44 days. After leaching with distilled water, insoluble weathering products remaining on the test specimens were examined with a variety of spectroscopic techniques including transmission electron microscopy, electron energy loss spectroscopy, synchrotron-radiation X-ray photoelectron spectroscopy and X-ray absorption near-edge spectroscopy. In another experiment, semi-polished slabs of a mixed-sulfide ore containing 3% Sb were submerged in distilled water and the evolution of leachate chemistry was monitored over a period of 147 weeks. The results show that galvanic interaction plays an important role in dictating the extent of Sb leaching under both subaerial and subaqueous conditions. Thus, detailed mineralogical characterization is indispensable in predicting the leaching of Sb from mine wastes containing mixed sulfides.

Additional Key Words: simulated weathering, sensitive surface analyses, galvanic sulfide oxidation.

---

[1] Paper presented at the 7th International Conference on Acid Rock Drainage (ICARD), March 26-30, 2006, St. Louis MO. R.I. Barnhisel (ed.) Published by the American Society of Mining and Reclamation (ASMR), 3134 Montavesta Road, Lexington, KY 40502

[2]Y.T. John Kwong and Allen Pratt are Research Scientists, CANMET Mining and Mineral Sciences Laboratories, Natural Resources Canada, Ottawa, ON K1A 0G1; Gianluigi Botton is Associate Professor of Materials Science, McMaster University, Hamilton, ON L8S 4M1.

7th International Conference on Acid Rock Drainage, 2006 pp 993-1006
DOI: 10.21000/JASMR06020993

https://doi.org/10.21000/JASMR06020993

Introduction

Stibnite is a common accessory mineral associated with silver mineralization. In Canada, for example, stibnite has been identified occurring in small amounts in both of the historic Cobalt and Keno Hill mining camps (Petruk, 1971; Lynch, 1989), which were respectively the largest and the second largest Canadian Ag producers to date. In the Eskay Creek mine, a major Au and Ag producer in the province of British Columbia, stibnite is a major sulfide mineral in the ore (Biles et al., 2000). In these deposits, stibnite is closely associated with other sulfides, sulfosalts and arsenides such as galena, sphalerite, pyrite, tetrahedrite, cobaltite and lőllingite. However, the rarity of stibnite relative to other common sulfide minerals has resulted in little work done to elucidate its weathering behavior. It is believed that acidic conditions have to be generated by the oxidation of other associated sulfides before antimony can be leached from stibnite (Boyle and Dass, 1971). However, at the Eskay Creek mine, fresh tailings and waste rock have been immediately disposed of in a lake to suppress sulfide oxidation and yet an increase in dissolved Sb concentration in the lake water has been noted since the commencement of mining (H.A. Simons Ltd., 1999). It has been suggested that stibnite is the main source of the released Sb (W.A. Price, personal communication, December 1, 2001).

Antimony is considered a heavy metal non-essential for optimal functioning of biological processes in an organism which, at high concentrations, is more toxic than As and Pb (Reimann and Caritat, 1998). The leaching of Sb from Sb-containing minerals and rocks may therefore have important ecotoxicological implications. To elucidate the geochemical behavior of stibnite under ambient conditions, simulated weathering has been conducted on polished slabs cut from a museum-grade stibnite specimen and on Eskay Creek ore specimens containing significant amounts of stibnite. Following a brief description of the experimental methods and presentation of the test results, the implications of the findings for metal leaching from sulfides and sulfosalts containing Sb are discussed.

Experimental Methods

Two series of experiments were conducted to elucidate the leaching of Sb from Sb-containing minerals and rocks. The first experiment focused primarily on the effects of exposing the test materials to moist air. Part 1 of the experiment involved 37 days of accelerated weathering of a polished slab (~15 mm x 15 mm x 5 mm) of museum-grade stibnite in an enclosed chamber (Fig. 1) with 100% humidity at 30.3±1.4^{o}C. The objective was to generate a weathered surface for detailed instrumental analyses using transmission electron microscopy (TEM) and electron energy loss spectroscopy (EELS). Part 2 of the experiment involved short-term (44 days) accelerated weathering at 35.2±2.0^{o}C of semi-polished slabs of stibnite and four ore specimens enriched in Sb. At the end of the accelerated weathering, the specimens were soaked in distilled water for two hours for determination of leached metals prior to air-drying overnight for examination under a petrographic microscope and a scanning electron microscope equipped with an energy-dispersion X-ray analyzer. A sample showing prominent pyrite inclusions in stibnite was selected for detailed surface analysis using synchrotron-radiation X-ray photoelectron spectroscopy (SR-XPS) and X-ray absorption near-edge spectroscopy (XANES). The collected leachates were analyzed by inductively coupled plasma atomic emission spectroscopy (ICPAES) or mass spectroscopy (ICPMS).

Figure 1. Setup of weathering chamber used in the simulated weathering experiments.

The second experiment simulated long-term (3 years) weathering of a Sb-bearing, mixed-sulfide ore submerged under water. Three semi-polished slabs, each measuring approximately 15 mm x 15 mm x 5 mm, were immersed in 15 ml of distilled water in three 20-ml glass beakers, giving rise to a water cover of about 1 cm deep. These beakers carrying the test samples and another two with distilled water only as running blanks were stored in a covered weathering chamber (Fig. 1) at room temperature (26.9±3.2^{o}C). Through the course of three years of simulated weathering, the standing water in each beaker was replaced four times and analyzed by ICPAES and ICPMS for a suite of dissolved constituents. From the leachate analyses, the cumulative releases of selected constituents were calculated and compared to assess the relative extent of metal leaching from the prevalent minerals.

Results and Discussion

Microbeam Analysis of Weathered Stibnite

With an unaided eye, except for a few scattered stained spots, the stibnite specimen appeared to have survived the 37 days of exposure to a warm (30^{o}C) and humid (100% relative humidity) environment with little alteration. Upon examination under a petrographic microscope, the tarnished spots were observed to be concentrated around local defects on the stibnite surface and in areas with rare pyrite inclusions. Figure 2 compares the photomicrographs of a selected area of the stibnite surface with a pyrite inclusion before and after the simulated weathering. It is apparent that preferential weathering of stibnite has occurred adjacent to pyrite. Using focused ion beam (FIB) imaging, the surface features of a tarnished area were also captured (Fig. 3). Focused ion beam (FIB) instruments operate in a similar manner to a scanning electron

microscope except that they use a finely focused beam of gallium ions that can be operated at low beam currents for imaging or high beam currents for site-specific sputtering or milling. A detailed introduction to FIB is provided in Phaneuf (1999). Figure 3C shows that secondary, acicular (needle-shaped) precipitates abound in the tarnished areas. To characterize the detailed composition of these altered surfaces and secondary precipitates by TEM, thin slices were cut from the specimen with the FIB perpendicular to the areas of interest. Prior to the FIB sample preparation, the area of interest on the target surface was protected from the ion-beam damage by coating with a thin film of palladium. Figure 4 shows the distribution of Fe, Sb and O in the cross-section containing the stibnite-pyrite interface. It is evident that adjacent to pyrite, stibnite has been replaced by a Sb-O phase. The elemental maps of a slice containing an acicular precipitate are shown in Fig. 5. Figure 6 compares the EELS O K-edge spectra of the relatively fresh stibnite, the secondary Sb-O phase at the interface of pyrite and stibnite, and the secondary precipitates found on the tarnished stibnite surface. Apparently, the acicular precipitates have a similar composition as the secondary Sb-O phase and the underlying stibnite is relatively unaltered.

It should be noted that, after the simulated weathering, the surface of the interior portion of the pyrite grain was also partly tarnished, indicative of alteration (Fig. 2, right). Detailed examinations under a petrographic microscope and a SEM showed that the tarnish was caused by small amounts of stibnite included in the pyrite, which were preferentially weathered in the process.

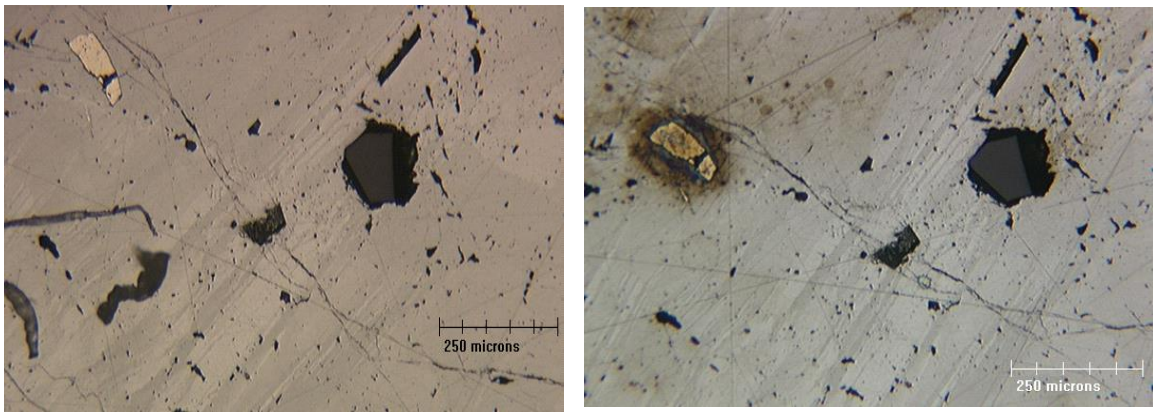

Figure 2. Photomicrographs of a selected area on the stibnite surface showing an included pyrite (top left corner in both pictures) before (left picture) and after (right picture) the simulated weathering.

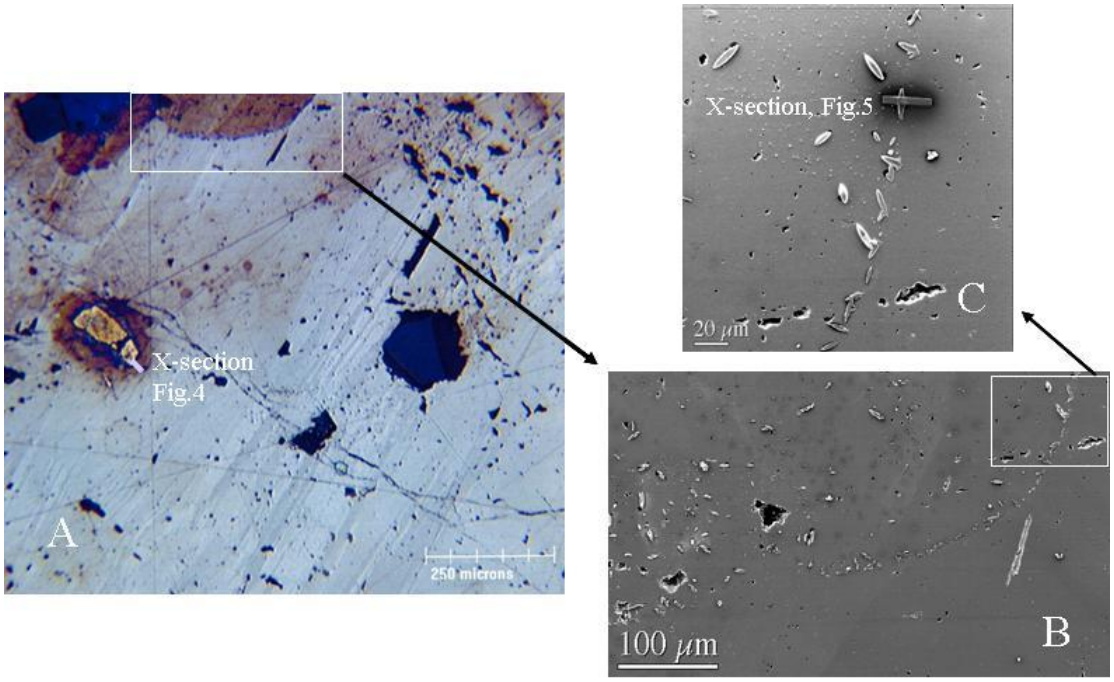

Figure 3. FIB images (B, C) of a tarnished area (white rectangle) in the photomicrograph of the weathered stibnite (A) showing a concentration of small, needle-like crystals in the tarnished spot, especially along its perimeter. C is an enlargement of the marked area in B. Cross sections at marked locations in A and C are detailed in Figures 4 and 5 below.

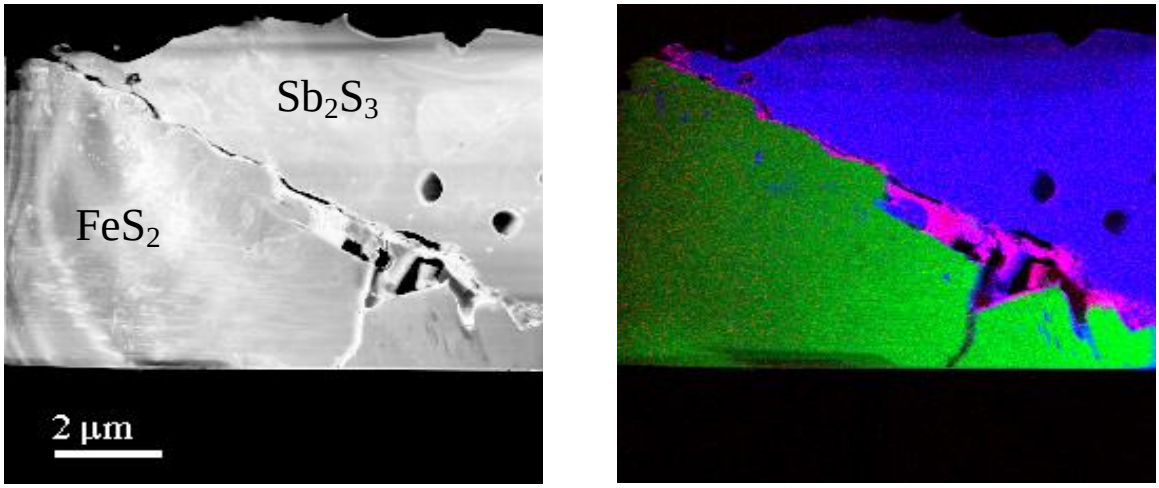

STEM ADF image EDS map: R=O, G=Fe, B=Sb

Figure 4. An electron photomicrograph acquired by a scanning transmission electron microscope in annular dark-field mode (STEM ADF image, left) and the corresponding X-ray map of the same area (EDS map, right) showing the distribution of Fe, O and Sb across the pyrite-stibnite interface. The map is color coded with green, red and blue representing Fe, O and Sb, respectively.

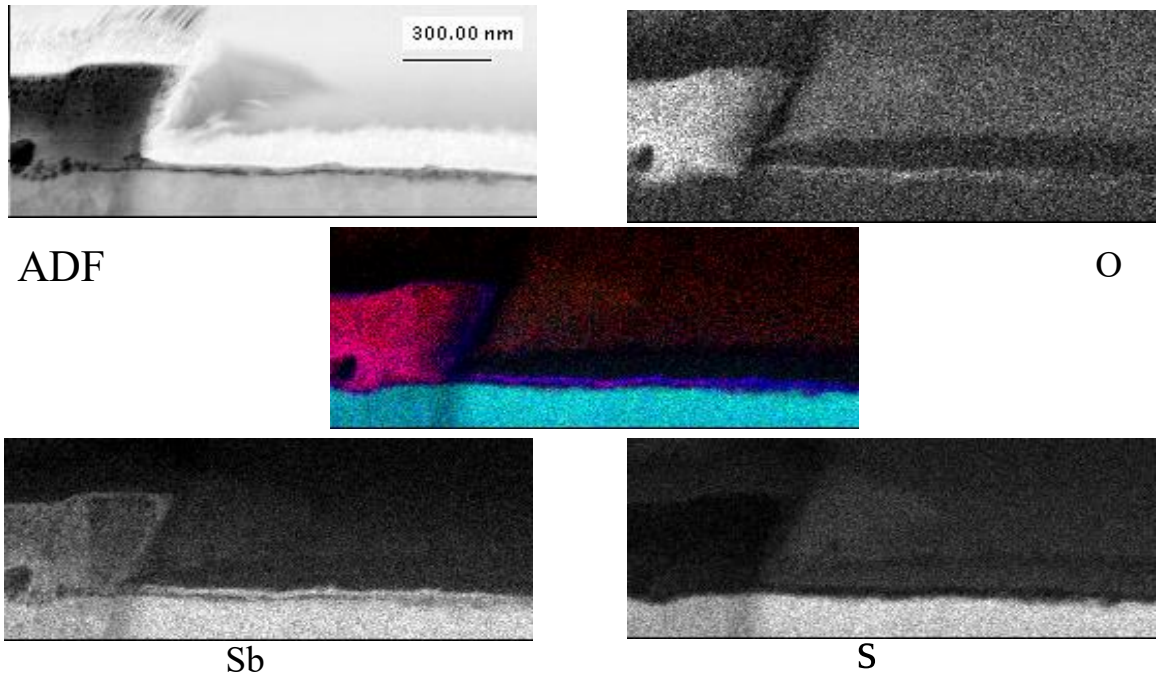

Figure 5. Elemental map of a cut slice containing an acicular precipitate on stibnite depicted in Fig.3. (For comparison with the stibnite-pyrite interface shown in Fig.4, the same color scheme is used in the middle diagram to depict the elemental distribution).

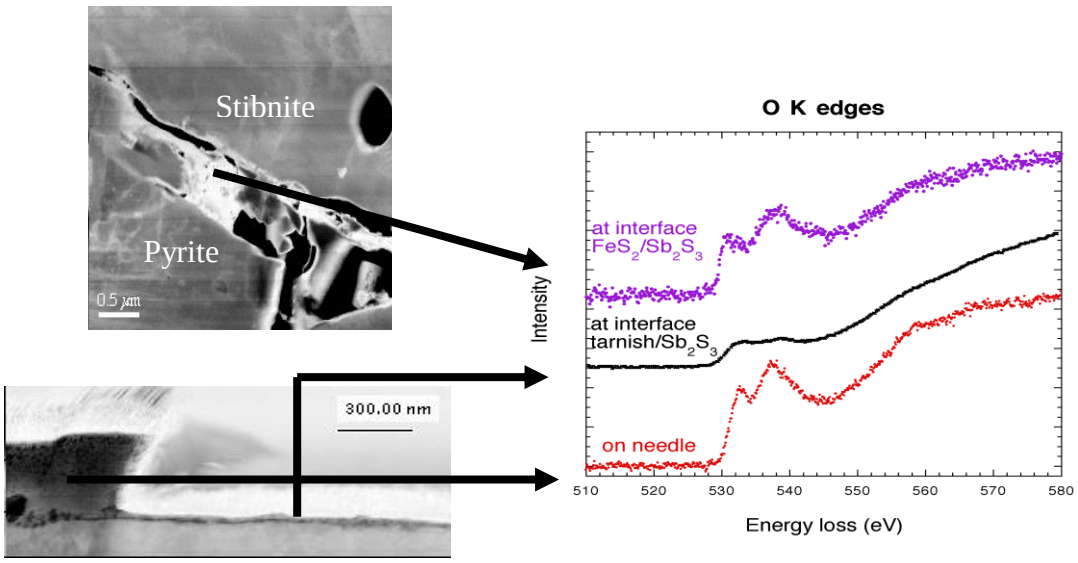

Figure 6. A comparison of the O K-edge spectra of the altered material at the pyrite-stibnite interface, the acicular precipitates and the underlying stibnite, showing that the weathering product is enriched in oxygen.

Leaching and Characterization of Stibnite and Sb-rich Ore Specimens after Accelerated Weathering

From the leachate analyses, the net releases of elements of interest from the semi-polished slabs of stibnite and Sb-containing mixed-sulfide ores after 44 days of accelerated weathering at 35°C are calculated per unit mass of the specimens tested. These are compared in Table 1 with their initial concentrations in the test specimens.

Table 1. Amount of selected elements remobilized after 44 days of accelerated weathering compared with their original concentration in the test specimens.

Element	Stibnite		Ore 1		Ore 2	
	Initial(%)	Leached(µg/kg)	Initial(%)	Leached (µg/kg)	Initial(%)	Leached[1](µg/kg)
As	nd[2]	46.0	0.06	177	0.08	4.34 ± 2.09
Cu	nd	3.24	0.54	174	4.04	8.44 ± 9.64
Fe	nd	<0.1	0.51	<0.1	3.02	<0.1
Pb	nd	61.4	1.20	<0.1	6.39	1410 ± 960
Sb	71.7	2710	28.3	2540	2.96	285 ± 127
Zn	nd	246	11.3	246	11.3	13100±21300

[1]Average of three samples tested; [2]nd = not determined

It is apparent from the data shown in Table 1 that the amount of metals/metalloids leached bears little relation to their original concentration in the test samples. For example, although stibnite contains two and a half times more Sb than the mixed-sulfide Ore 1, the amounts of Sb leached from both specimens are similar. On the other hand, although both Ore 1 and Ore 2 have the same initial Zn concentration, the amount of Zn leached from Ore 2 is two orders of magnitude higher than that from Ore 1. Stibnite, tetrahedrite, sphalerite, galena and pyrite are the main sulfide minerals occurring in both of the ore samples. In addition to differences in the relative abundance of stibnite and tetrahedrite (more abundant in Ore 1), galena and pyrite (more abundant in Ore 2), the two ores also differ in chalcopyrite content. Chalcopyrite has been observed only in Ore 2. The three tested specimens of Ore 2 gave leachates with a highly variable chemistry. This either reflects the heterogeneity of the collected bulk ore sample or local controls of metal/metalloid leaching by the prevalent mineral assemblages.

In view of the observations made by TEM examination of the weathered stibnite specimen and the highly variable leachate chemistry acquired in the second short-term weathering experiment, the Ore 1 specimen was selected for detailed SR-XPS and XANES analyses. Attention was focused on an area of the specimen where stibnite is in direct contact with pyrite (Fig. 7). The analyses were conducted at Beamline 7.3.1.2 of the Advanced Light Source at the Lawrence Berkeley Laboratory in California.

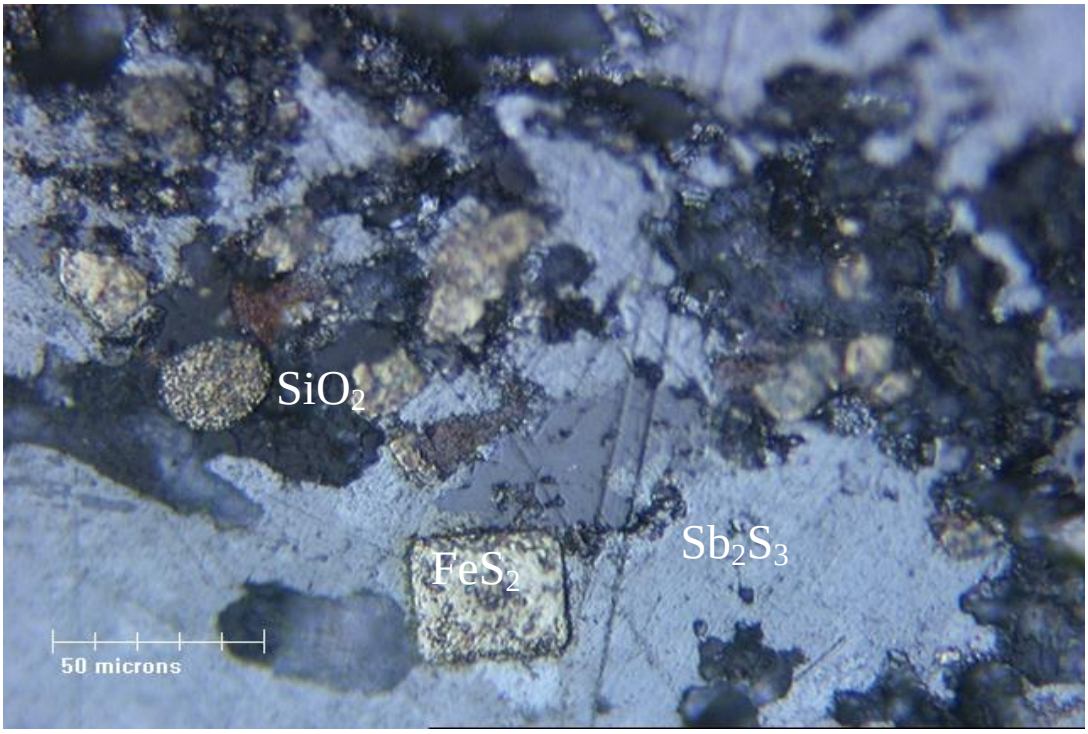

Figure 7. Photomicrograph of specimen Ore1, showing pyrite surrounded by stibnite.

Figure 8 shows the SR-XPS and XANES spectra of a spot in pyrite surrounded by stibnite in Ore 1. XPS is a sensitive surface-analytical technique that can render detailed information on the elemental composition of a mineral surface as well as the oxidation states and bonding partners of the constituent elements. The analysis depth of XPS is generally in the range of 1 to 3 nm whereas the penetration depth of XANES generally ranges from 30 to 40 nm. Thus, the latter reveals more detailed information on the bulk composition and oxidation states of a mineral under investigation. Comparing the SR-XPS and XANES spectra obtained from a spot inside the occluded pyrite, it is evident that the interior of the sulfide mineral is unaltered but the surface is covered by a thin film of Sb oxide. The surface oxide layer practically concealed the underlying pyrite in the SR-XPS analysis such that little signal for Fe was detected. It is not clear whether the Sb oxide of unknown composition had formed as a direct oxidation product of stibnite or was deposited from solution when the sample was dried for synchrotron analysis.

The results of spot analyses on stibnite adjacent to the pyrite grain are shown in Fig. 9. The XANES data are compatible with the TEM-EELS analyses that a small amount of oxygen was present in the analyzed spot, presumably restricted to the surface. Admittedly, XANES is not a surface-analysis technique. However, the bulk matrix is sulfide and contains no oxygen. The only place the detected O can originate from is an oxygen-bearing species on the surface. From a traverse of spot analyses from the interior of pyrite well into the surrounding stibnite, it became clear that oxygen is more concentrated at the pyrite-stibnite interface. The preferential weathering of stibnite at the contact zone is schematically shown in Fig. 10. Such a weathering pattern is typical of galvanic interaction between contacting sulfides with contrasting electrode potentials.

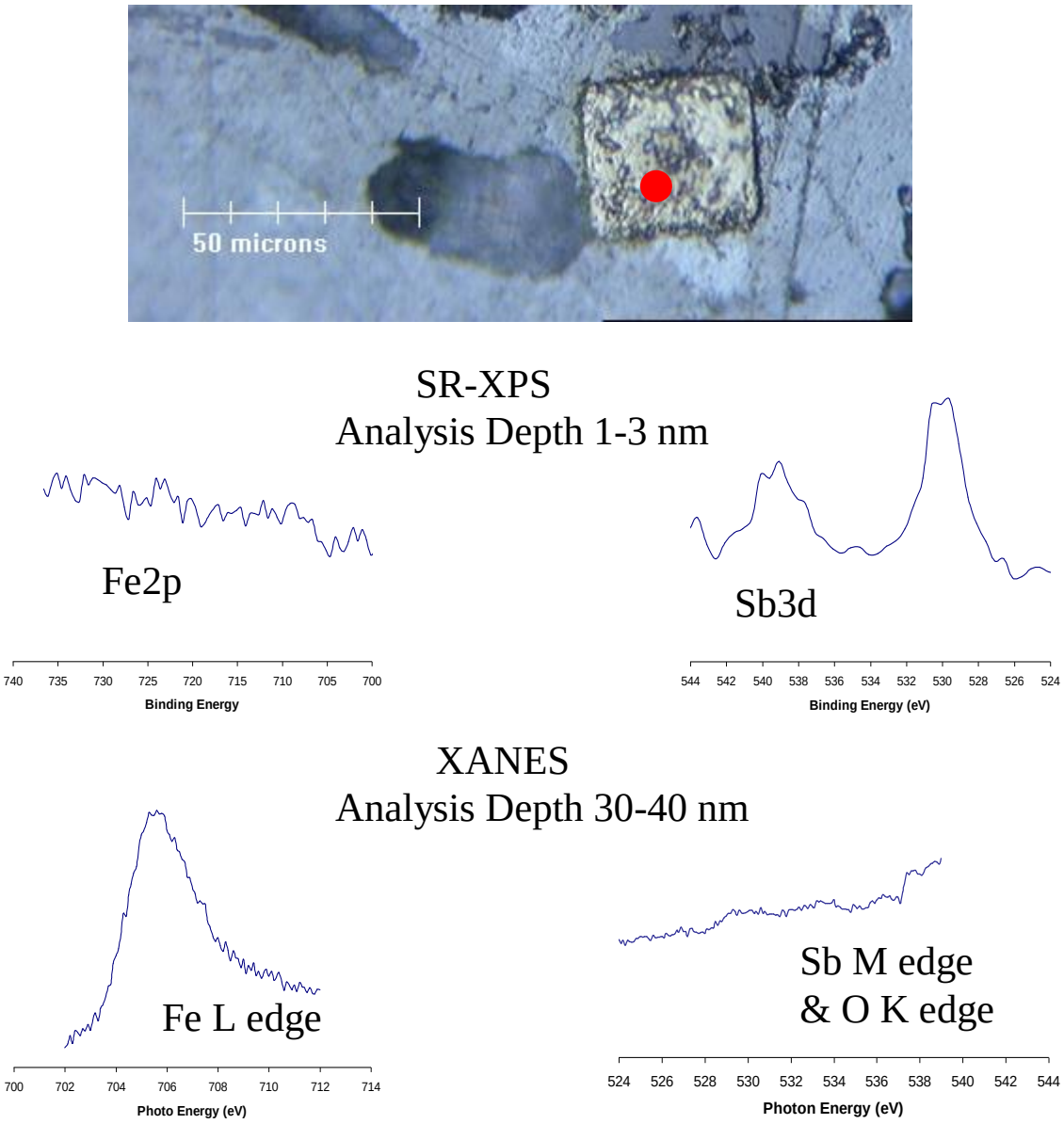

Figure 8. Spot SR-XPS and XANES analyses of pyrite (red dot) surrounded by stibnite.

Galvanic sulfide oxidation is a naturally-occurring metal-leaching mechanism driven by the potential difference between two contacting sulfides. It leads to preferential oxidative dissolution of the sulfide with a lower electrode potential while the other with a higher electrode potential is protected from oxidation. Interested readers are referred to Kwong et al. (2003) and Abraitis et al. (2004) for a brief review of the theory, practical examples and implications of galvanic sulfide oxidation.

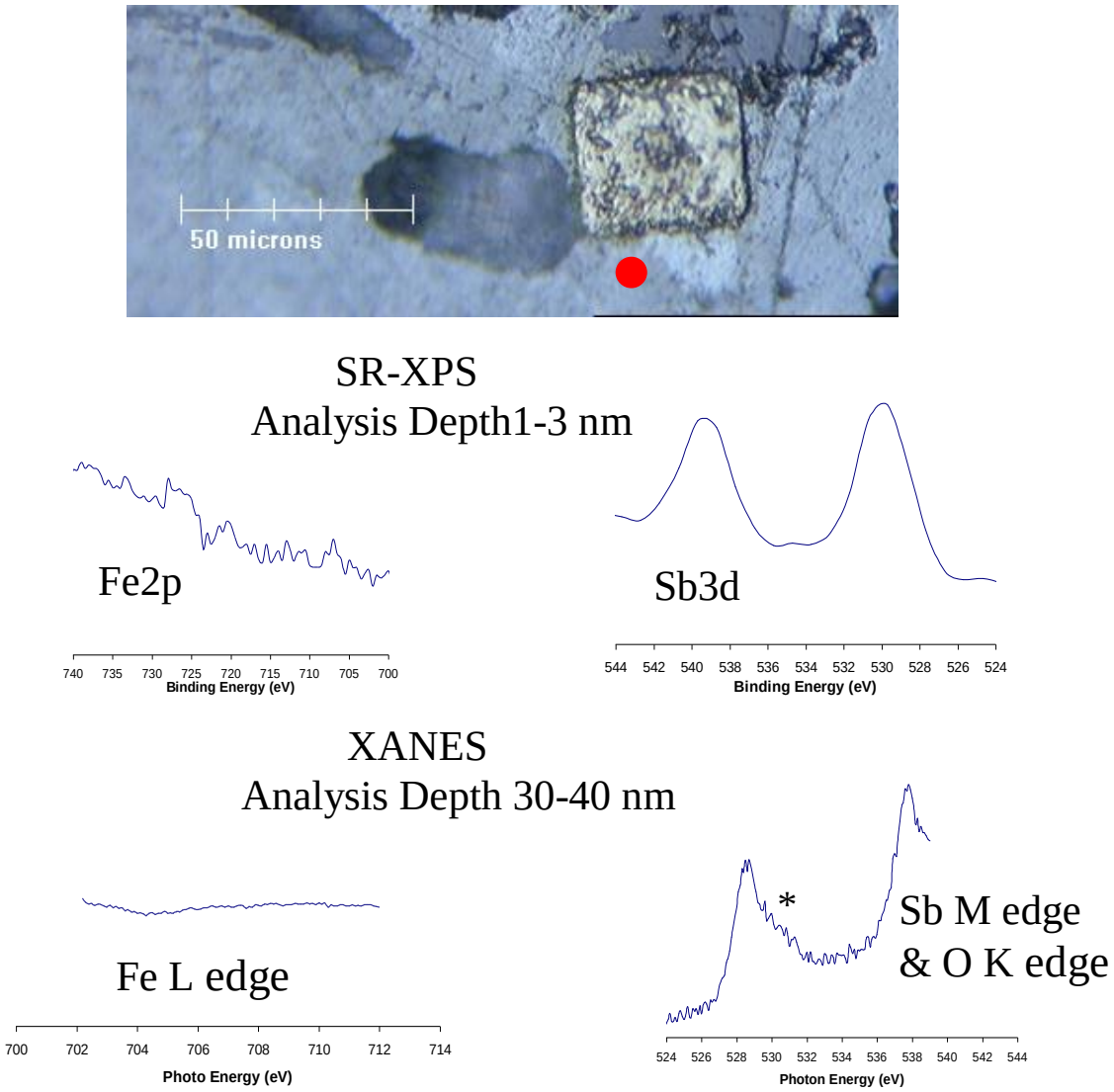

Figure 9. Spot SR-XPS and XANES analyses of stibnite adjacent to pyrite in Ore 1. The asterisk (*) in the bottom right XANES spectrum shows the position of the O K edge. The resolution in the corresponding SR-XPS spectrum is too coarse to reveal the overlapping Sb3d and O K edge peaks.

If galvanic sulfide oxidation was indeed the dominant process controlling metal/metalloid leaching from the weathered specimens, then the apparently confusing leachate chemistry (Table 1) can readily be interpreted in terms of the differing mineralogy of the test samples. The TEM, EELS, SR-XPS and XANES analyses clearly demonstrate preferential oxidative dissolution of stibnite adjacent to pyrite. The small amounts of dissolved As, Cu, Pb and Zn detected in the stibnite leachate, are likely derived from trace elements associated with the mineral. As reflected by the low Fe content (Table 1), pyrite is relatively rare in Ore 1. This sparseness has hampered the preferential weathering of galena and sphalerite, both of which have low electrode potentials

compared with that of pyrite (Kwong et al., 2003). Consequently, insignificant amounts of Pb and Zn have been released to the leachate. In the absence of chalcopyrite in Ore 1, the minor solubilization of As and Cu is likely due to the weathering of tetrahedrite. With the Ore 2 specimens, the presence of more pyrite has led to the release of orders of magnitude more Pb and Zn into solution upon post-weathering leaching. In contrast, the subdued release of Sb indicates that either stibnite has a higher electrode potential than galena and sphalerite or that pyrite is in more frequent contact with galena and sphaerite than with stibnite in the test specimens.

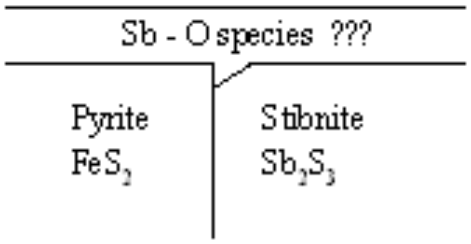

Figure 10. A schematic diagram illustrating the synopsis of SR-XPS and XANES analyses. Stibnite is apparently preferentially weathered adjacent to pyrite with the resultant thickened deposit of a secondary antimony oxide at the interface.

Antimony Leaching from Sb-rich Specimens under a Shallow Water Cover

Both of the short-term simulated weathering experiments were conducted under subaerial conditions. To investigate the leaching of Sb under a shallow water cover, the three Ore 2 specimens, which average 2.96% Sb, were used in the long-term, under-water weathering experiment. The net release of selected elements to the water cover after three years of simulated weathering at room temperature is depicted in Fig. 11. To allow data presentation on a log scale, the cumulative releases of all selected elements are arbitrarily set at a negligible value (0.001 mg/kg) on Day 0. The plotted data are average values of those measured individually from the three test specimens. The leachate pH has remained near neutral (7.0 ± 0.3) throughout the experiment.

It is evident from Fig. 11 that the evolution curves for the cumulative release of Pb, S (as sulfate in solution) and Zn are similar, suggesting that the three elements have been released into solution through oxidative dissolution of galena and sphalerite. The releases of Cd and Sb are three to four orders of magnitude lower than those of Pb and Zn. Cadmium is a minor constituent of the ore samples and is likely associated with sphalerite. The low concentration of dissolved Cd in the leachate is therefore expected. However, the concentration of Sb in the ore samples is only about half that of Pb and one fourth that of Zn (2.96%, 6.39% and 11.3%, respectively). The orders of magnitude smaller Sb release compared with those of Pb and Zn suggests that the Sb-containing minerals, namely stibnite and tetrahedrite, have reacted much more slowly than galena and sphalerite. If galvanic interaction with pyrite is the dominant process that leads to oxidative dissolution of the sulfides concerned during the simulated weathering, then the smaller release of Sb relative to Pb and Zn indicates that stibnite and tetrahedrite probably have a higher electrode potential than those of galena and sphalerite. This follows from the fact that galvanic sulfide oxidation is driven by the potential difference between

the contacting sulfides (Kwong et al., 2003). The smaller the difference in electrode potential between two contacting sulfides, the less intense is the galvanic interaction between the minerals and hence the slower the oxidative dissolution of the mineral with the lower electrode potential.

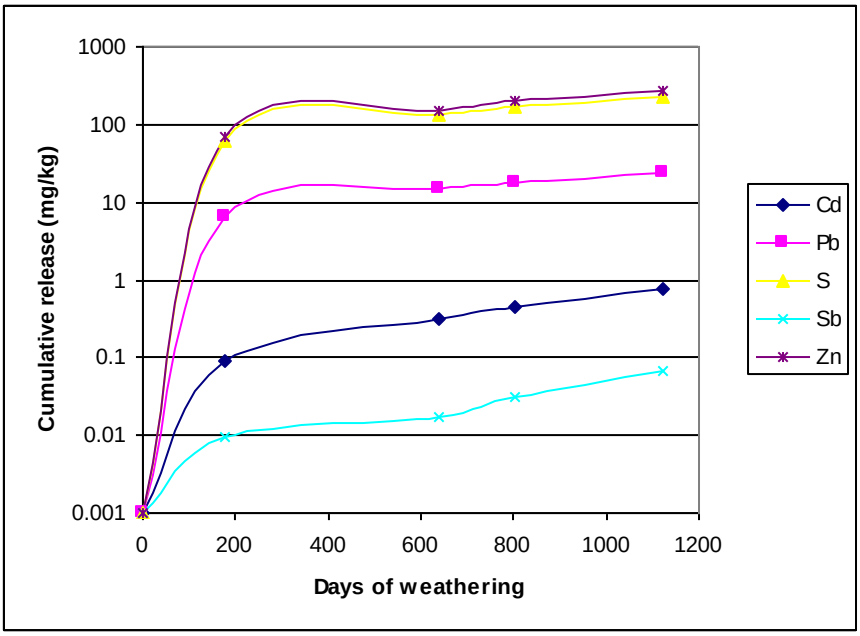

Figure 11. Cumulative releases of Cd, Pb, S, Sb and Zn during a three-year simulated weathering of Sb-rich specimens under a shallow water cover.

It should also be noted in Fig. 11 that the cumulative release of Pb and Zn becomes asymptotic (i.e., tends to level off) towards the end of the weathering experiment whereas the release of Sb shows a continuous increasing trend. This observation can readily be explained in terms of galvanic interaction. The effect of galvanic sulfide oxidation is most prominent at the interface of the contacting sulfides (Kwong et al., 2003). As preferential dissolution of the anode sulfide (the one with a lower electrode potential) continues, the contact with the cathode sulfide will eventually break off, short-circuiting the galvanic cell. When this happens, the metal release to the solution will be solely dictated by the sulfide solubility, which is negligible under ambient, near-neutral pH conditions. Probably, such a case has taken place with the pyrite-galena and pyrite-sphalerite couples in the weathering experiment. Contacts between the sulfide pairs have largely been broken after three years of continuing, preferential weathering of galena and sphalerite in contact with pyrite so that galvanic interaction is no longer active towards the end of the simulated weathering under a shallow water cover. Because of the slower reaction between pyrite and stibnite/tetrahedrite, the galvanic interaction between the sulfide pair(s) remains strong at the end of the simulated weathering. However, resorption of some Sb in the form of oxides on mineral surfaces as inferred from the synchrotron-based analyses in the subaerial weathering experiment may have also reduced the net release of Sb into solution.

As mentioned above, chalcopyrite has been detected in the Ore 2 specimens used in the weathering experiments. However, with an electrode potential very close to pyrite (Kwong et

al., 2003), chalcopyrite is also galvanically protected from oxidative dissolution when in contact with galena, sphalerite, stibnite and tetrahedrite. The trace amount of Cu released to solution (not plotted) is most likely derived from oxidative dissolution of tetrahedrite.

Conclusions

Petrographic examination and profiling of surface chemistry by the instrumental techniques have demonstrated preferential weathering of stibnite adjacent to pyrite. The leachate chemistry acquired in both the subaerial and subaqueous weathering experiments affirmed potential partial resorption of some of the released Sb. Overall, the experimental results strongly suggest that galvanic interaction is an important mechanism for preferential leaching of Sb. In addition to environmental parameters such as pH, Eh and availability of oxygen and moisture, the composition and nature of the closest neighbor also significantly affect the rate and extent of oxidation of stibnite and tetrahedrite in a mixed mineral assemblage.

Acknowledgements

The authors thank G.D. Ackerman of the Advanced Light Source, Berkeley, for assistance in synchrotron analyses. Internal review of the draft manuscript has been kindly furnished by J. Zinck and S. Beauchemin of the CANMET Mining and Mineral Sciences Laboratories. Referee comments provided by J. Jambor and H. Jamieson have helped to improve both the presentation and content of this paper.

Literature Cited

Abraitis, P.K., R.A.D. Pattrick, G.H. Kelsail and D.J. Vaughan. 2004. Acid leaching and dissolution of major sulphide ore minerals: processes and galvanic effects in complex systems. Mineralogical Magazine 68:343-351.http://dx.doi.org/10.1180/0026461046820191.

Biles, C., K. Loughran, and D. Milojkovic. 2000. Homestake Canada Inc. – Eskay Creek Mill. *In*: B. Damjanovic and J.R. Goode (eds.), Canadian Milling Practice. Canadian Institute of Mining, Metallurgy and Petroleum, Special Volume 49, p.26-30.

Boyle, R.W. and A.S. Dass. 1971. The geochemistry of the supergene processes in the native silver veins of the Cobalt-South Lorrain area, Ontario. *In*: Berry, L.G. (ed.), The Silver-Arsenide Deposits of the Cobalt-Gowganda Region, Ontario. Canadian Mineralogist **11**:358-390.

H.A. Simons Ltd. 1999. Albino Lake Water Quality Model Phase III. Report prepared for Homestake Canada Inc., May, 1999.

Kwong, Y.T.J., G.W. Swerhone and J.R. Lawrence. 2003. Galvanic sulphide oxidation as a metal-leaching mechanism and its environmental implications. Geochemistry: Exploration, Environment, Analysis 3:337-343.http://dx.doi.org/10.1144/1467-7873/03/013.

Lynch, J.V.G. 1989. Large-scale hydrothermal zoning reflected in the tetrahedrite-freibergite solid solution, Keno Hill Ag-Pb-Zn district, Yukon. Canadian Mineralogist **27**:383-400.

Petruk, W. 1971. General characteristics of the deposits. In: Berry, L.G. (ed.), The Silver-Arsenide Deposits of the Cobalt-Gowganda Region, Ontario. Canadian Mineralogist **11:**76-107.

Phaneuf, M.W. 1999. Applications of focused ion beam microscopy to materials science specimens. Micron 30:277-288.http://dx.doi.org/10.1016/S0968-4328(99)00012-8

Reimann, C. and P. de Caritat. 1998. Chemical elements in the environment – Factsheets for the Geochemist and Environmental Scientist. Springer-Verlag Berlin Heidelberg.